PERGAMON

International Journal of Solids and Structures 37 (2000) 2185–2214

INTERNATIONAL JOURNAL OF SOLIDS and STRUCTURES

www.elsevier.com/locate/ijsolstr

A viscoplastic approach to model the flow of granular solids

Sergio A. Elaskar[a], Luis A. Godoy[a,*], Donald D. Gray[b], James M. Stiles[b]

[a]*Engineering School, National University of Córdoba and CONICET, P.O. Box 916, Córdoba 5000, Argentina*
[b]*Civil and Environmental Engineering Department, West Virginia University, Morgantown, WV 26506-6103, USA*

Received 6 February 1998; in revised form 16 October 1998

Abstract

The flow of granular solids within rigid walls is modeled using continuum mechanics. The problem is represented as a viscoplastic flow in which the discontinuity function is taken as in previous works by Gray and Stiles, while the flow rule is modeled by the von-Mises criterion. The resulting model is incompressible and based on non-associated viscoplasticity. The apparent viscosity results in a non-linear function of the second invariant of the symmetric rate of deformation tensor and of the pressure. Friction, cohesion and fluidity of the granular model are taken into account. The constitutive model has been implemented assuming steady-state, in which the granular material flows under a critical state (incompressible behavior). Discretization of the problem has been carried out by finite elements, with direct iteration techniques to solve the non-linear system of equations. The model has been applied to the massive flow of granular material stored in vertical silos and hoppers with axisymmetric or planar shape. Comparisons with experimental tests performed by other authors are presented, together with parametric investigations to identify the main variables affecting the response.

1. Introduction

Interest in the modeling of the flow of granular solids has been stimulated in recent years by a number of problems, such as the discharge of grains stored in silos, the manipulation of coal and other minerals, the transport of sediment in rivers and oceans, etc.

There are several ways to model the flow of granular solids using mechanical sciences: (a) two-phase flow in which the particles have a dynamic influence from drag stresses due to interstitial fluid (Syamalal, 1985); (b) rapid unfluidized flow in which the stresses due to collisions between particles are

* Corresponding author. Structures Department, National University of Córdoba, P.O. Box 916, Córdoba 5000, Argentina. Tel.: 54-351-4334145; fax: 54-351-4334144.

E-mail address: lgodoy@com.uncor.edu (L.A. Godoy)

0020-7683/00/$ - see front matter
PII: S0020-7683(98)00300-X

dominant, as in models based on kinetic theories (see, for example, Lun et al., 1984; Johnson and Jackson, 1987; Savage, 1988; Ocone and Astarita, 1995); and (c) cohesive and frictional flow, which is the subject of this paper.

Furthermore, there are several ways to carry out the analysis of cohesive and frictional flows, i.e. discrete particles; micromechanics; and phenomenological models. In particle analysis one models the evolution of a set of particles which are interrelated and each particle should satisfy the condition of conservation of linear and angular momentum (Cundall and Strack, 1979; Potatov and Campbell, 1994). Because the contacts are modeled, this simulation requires massive computing facilities to track the position of each particle during the flow. In the micromechanics approach the granular material is considered as a continuum, but the constitutive equation is obtained from the microscopic behavior and from the properties of the individual grains (Mehrabadi, 1986). Finally, continuum mechanics is employed in a phenomenological approach, as in Diez and Godoy (1992), Elaskar et al. (1996), Elaskar and Godoy (1998a), Gray and Stiles (1991), Haussler and Eibl (1984) and Lade (1977). This work falls within the phenomenological approach, based on continuum mechanics.

Early work in this field was done by Jenike and co-workers, for frictional materials, using analytical tools. The solution was limited to simple geometries and material properties. More general models can be achieved in several ways:

(a) Plastic flow of solids: these are continuum models which are used in plasticity theory to model the deformations of the bulk material. Examples are shown by Gray et al. (1991), Haussler and Eibl (1984) and Kolymbas (1994). The transient response at the beginning of the flow requires an extremely fine step to achieve meaningful results. Large strain plasticity models should be introduced if one attempts to investigate the flow until it reaches a steady-state.
(b) Viscoplastic flow of a non-Newtonian fluid: as in the first group, this model employs continuum mechanics, but with the advantage that both the transient response and the steady state can be investigated at once. The material properties of cohesion, friction and fluidity are combined to obtain an apparent viscosity, which also depends on the local values of pressure and velocity of the flowing granular solid. A steady state analysis has been implemented by Diez and Godoy (1992). In its original version, the viscoplastic model used a non-associative rule, with Drucker–Prager discontinuity surface and von-Mises criteria for the plastic potential. Numerical problems have been detected in this formulation, namely lack of convergence of the solution in some cases when direct iteration is used to solve the non-linear problem. Modifications introduced in this model were discussed by Elaskar et al. (1996), but showed some limitations. Thus, a new constitutive model is explored in this work, using a discontinuity surface due to Gray and Stiles (1988, 1990, 1991) and Gray et al. (1991), but adapted to the case of critical flow; and a von-Mises (incompressible) flow rule. The resulting model is based on non-associative plasticity (see, for example, Lade, 1977). The constitutive model has been implemented assuming steady-state flow, in which the granular material flows under a critical state (incompressible behavior).

In Section 2 we introduce a summary of the plastic discontinuity function employed in the model, as presented in Gray et al. (1991). Such a function is employed in the viscoplastic formulation of Section 3, which is writen in the form of viscoplasticity originally due to Perzyna (1966). The apparent viscosity results in a non-linear function of the second invariant of the symmetric rate of deformation tensor and of the pressure. The discretization in terms of finite elements is described in Section 4, together with the numerical techniques employed for the solution of the non-linear problem. Comparisons with experiments carried out by other authors, as well as with independent numerical results, are presented in Section 5. Results of numerical experiments for two-dimensional and axisymmetric problems are presented in Section 6, to illustrate how the variables of the constitutive model affect the response in

terms of pressures and velocities. The general procedure employed to simulate the discharge of silos is discussed in Section 7. The main conclusions of the study are summarized in Section 8.

2. Plastic discontinuity function

In this section we review some basic aspects of a model for the flow of granular materials with cohesion and friction proposed by Gray et al. (1991). The model is based on continuum mechanics and the theory of plasticity and considers a rigid-plastic behavior. The constitutive model includes to main aspects: the discontinuity function and the plastic potential. In its original version, this model of plastic flow is based on an associated rule, in which the same function is employed for the plastic potential and the discontinuity surface.

The plastic discontinuity function is here denoted by $F(T_i, \xi)$ and the condition

$$F(T_i, \xi) = 0$$

represents a surface in the Haigh–Westergaard space of principal stresses; where T_{ij} are the components of the stress tensor. The definition of such a surface may also be comprised of a set of internal variables ξ. For a rigid-plastic material, stress states represented on the inner volume enclosed by the discontinuity surface are associated to rigid behavior; while those on the surface are under plastic flow.

The components of the symmetric rate of deformation tensor D_{ij} are given by

$$D_{ij} = q\frac{\partial F}{\partial T_{ij}} \tag{1}$$

where q is a positive scalar and F is the discontinuity function (and also plastic potential). Thus, for small stresses the material is at rest and it flows under higher values of stresses.

Some experimentally observed features concerning the behavior of granular materials may be summarized as follows:

- The state representing the unloaded state should be inside or on the plastic discontinuity surface (see Gray et al., 1991). This means that the discontinuity function plotted in the space of principal stresses should cross the point of zero stress, or else that point should be inside the volume enclosed by the discontinuity surface.
- The onset of discontinuity of these materials is modified by the density. Thus, rather than having a unique discontinuity surface for a given material, there is a family of them depending on the density. The surface associated to the lowest density is contained inside those of higher densities (see Desai and Siriwardane, 1984).
- When flow is initiated, a bulk solid with low initial density tends to consolidate. On the other hand, a bulk solid with high initial density tends to expand. This process continues until the material reaches a critical state in which it flows with constant density (see Brown and Richards, 1970).

If the principal symmetric rate of deformation tensor components are plotted in the Haigh–Westergaard space, we notice that whenever there is consolidation of the material the projection of the symmetric rate of deformation vector on the hydrostatic axis is positive. When the material flows at a critical state then there is a null projection; whereas the projection becomes negative under dilatancy.

A constitutive model which satisfies the above requirements has been proposed by Gray et al. (1991). This is a generalization of the model by Pitman and Schaeffer (1987), in which a relation between the discontinuity function and the density of the material is established and the concept of critical state is

employed to identify the flow properties. Other constitutive models which incorporate those factors are reviewed for example by Desai and Siriwardane (1984).

The discontinuity surface can be written in the form

$$F = S_{II} + k^2(p + c)^m(p + c - 2p_c) = 0 \tag{2}$$

where S_{II} is the second invariant of the deviatoric stress tensor

$$S_{II} = \tfrac{1}{2}S_{ij}S_{ij} \tag{3}$$

$k = \sin\phi$; ϕ is the internal friction angle; p is the pressure in the granular solid; c is the cohesion of the material; the exponent m may take values in the range $0 < m \leqslant 2$; p_c is the pressure at the critical state and is related with the density ρ by

$$p_c = a\rho^{1/\beta} \tag{4}$$

in which a and β are material constants.

Eqn (2) represents a closed surface, with a vertex at $p = -c$ and another one at $p = 2p_c - c$. For $m < 1$ the critical state is closer to $p = -c$, while for $m > 1$ it is closer to $p = 2p_c - c$. The case $m = 1$

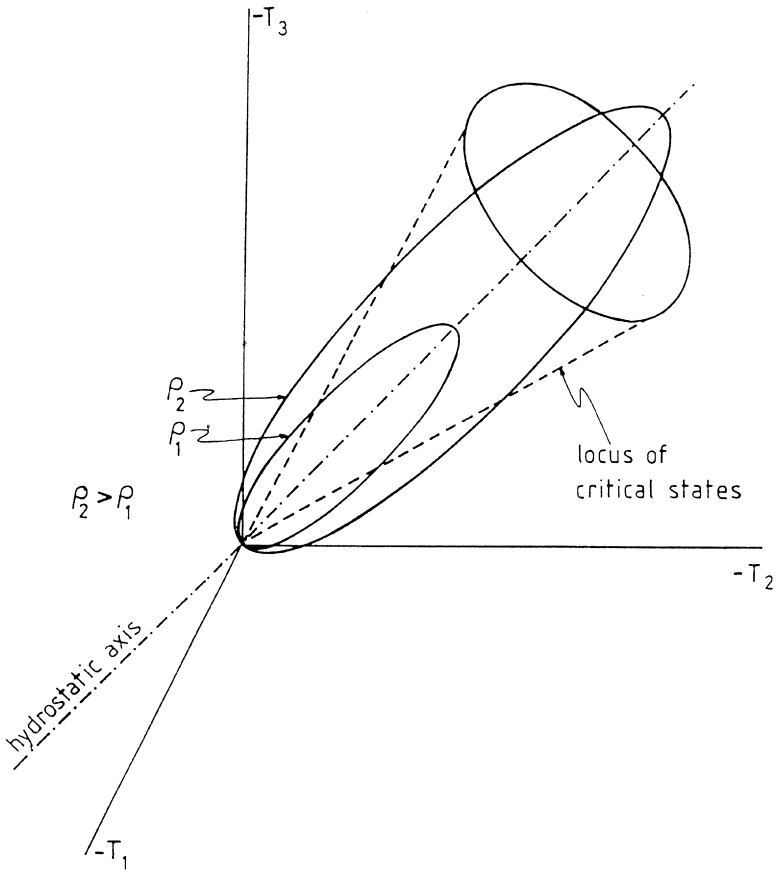

Fig. 1. Gray–Stiles discontinuity surface in the Haigh–Westergaard space ($c = 0$ and $m = 1$).

represents a symmetric surface and was first discussed by Gray and Stiles (1988). Fig. 1 illustrates the function of eqn (2) when $c = 0$ and $m = 1$.

For a given density, the intersection between the surface and an octahedral plane leads to a circular section with radius

$$r = k\sqrt{2\left[(p+c)^m(2p_c - c - p)\right]} \tag{5}$$

The largest value of the radius is

$$r_m = k\sqrt{\frac{2m^m(2p_c)^{m+1}}{(m+1)^{m+1}}} \tag{6}$$

and occurs at the pressure given by

$$p = \left(\frac{m}{m+1}\right)2p_c - c \tag{7}$$

The plots in Fig. 1 have been computed for $m = 1$ and different values of density. The locus of critical states is represented by a cone, which is the Drucker–Prager discontinuity surface. We shall employ this concept, but for values of $m \neq 1$.

For cases with zero cohesion, the discontinuity surface (2) reduces to

$$F = S_{II} + k^2\left(p^{m+1} - 2p^m p_c\right) = 0 \tag{8}$$

3. Viscoplastic model with non-associated plasticity

3.1. Discontinuity surface

In this section we concentrate on the constitutive model for steady-state flow of granular material under gravity action. Rather than looking at the flow using solid mechanics and plasticity, we proceed to carry out our investigation using non-Newtonian fluid mechanics and viscoplasticity (see Diez and Godoy, 1992; Flavigny and Nova, 1990). The following assumptions are made:

- During steady-state flow the material behaves as incompressible, or near-incompressible.
- The flow can be modeled using non-associated viscoplasticity.

The influence of compressibility of the material should be reflected in the constitutive equation. This has been discussed in detail by Elaskar and Godoy (1998a, b), in which numerical results show that the compressibility of the material only affects the results in extreme cases.

For an incompressible material under flow, the yield surface eqn (2) can be simplified. Incompressible behavior is only possible when the material has a deformation prior to the steady-state flow. It is assumed that this prior deformation occurs during the transient discharge. With a previous deformation it is acceptable to assume that the granular material flows in a critical state, so that the density is now constant. This is an incompressible flow.

The pressure is now a dynamic variable (see Aris, 1989). At the same time, the flow is incompressible only under critical conditions, with constant density, so that it is not necessary to distinguish between p_c and p in eqn (2).

The discontinuity function is thus modified to the form

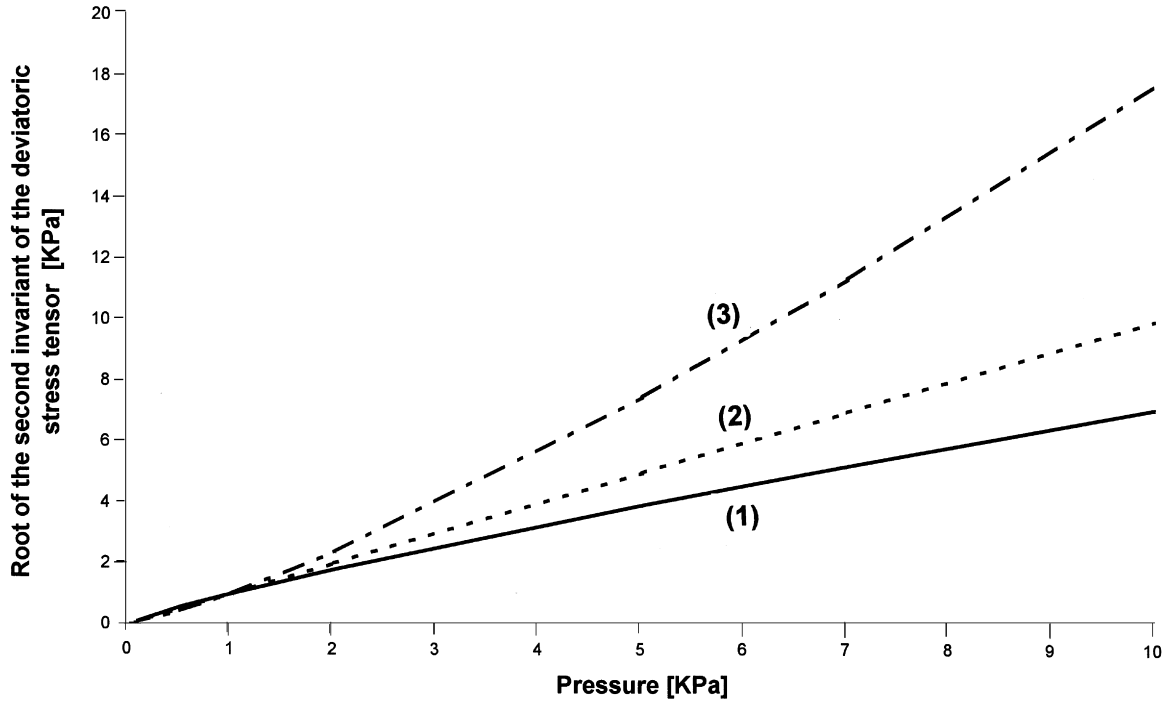

Fig. 2. Gray–Stiles discontinuity surface plotted in the meridian plane (1) $m = 0.7$, (2) $m = 1.0$, (3) $m = 1.5$.

$$F = S_{II} - k^2(p + c)^m(p - c) = 0 \tag{9}$$

which will be employed in the present work.

For a material with zero cohesion, eqn (9) reduces to

$$F = S_{II} - k^2 p^{(m+1)} = 0 \tag{10}$$

A plot of eqn (10) for different values of the exponent m is given in Fig. 2. This plot is the intersection between the discontinuity surface and a meridian plane in the Haigh–Westergaard space. Notice that for $m = 1$ we get the Drucker–Prager surface. For $m > 1$ and $p > 1$ kPa we get a surface on the exterior of Drucker–Prager. For $m < 1$ and $p > 1$ kPa the surface is inside the Drucker–Prager model. Thus, the exponent m plays an important role in the definition of what stress states are under plastic flow.

3.2. Viscoplastic constitutive equation

There are several theories for viscoplastic behavior, notably those due to Perzyna (1966) based on the theory of plasticity using internal variables (see Lubliner, 1990; Duvaut and Lions, 1972; Kolymbas, 1994). Here we follow the approach given by Perzyna, in which the general constitutive equation takes the form

$$D_{ij} = \gamma\langle F\rangle \frac{\partial Q}{\partial T_{ij}} \tag{11}$$

where $\langle\ \rangle$ are the Macauley brackets, i.e.

$$\langle F \rangle = F \quad \text{for } F > 0 \tag{12}$$

$$\langle F \rangle = 0 \quad \text{for } F \leqslant 0 \tag{13}$$

In eqn (11) F is the plastic flow function; Q is the plastic potential; γ is the fluidity.

Here we employ the flow condition of eqn (9), in which both cohesion and friction are taken into account. For the plastic potential we employ the von-Mises criteria, valid for an incompressible material.

$$Q = \sqrt{S_{II}} - k \tag{14}$$

Notice that if one employs another plastic potential, such as Drucker–Prager, then the material would not have incompressible behavior. This is clearly seen in the space of principal stresses, where the gradient of the von-Mises function is orthogonal to the hydrostatic axis while the derivative of Drucker–Prager is not.

The resulting formulation is based on non-associated plasticity. Such formulation is particularly adequate for incompressible flow of granular materials. In a formulation based on associated plasticity, on the other hand, one would find that the plastic potential depends on the first invariant of the Cauchy stress tensor. Further justification of the use of non-associated plasticity is given by other authors (see, for example, Lade, 1977).

Substitution of eqns (9) and (14) in the expression due to Perzyna (11) leads to

$$D_{ij} = \gamma \langle [S_{II} - k^2 (p+c)^m (p-c)] \rangle \frac{1}{2} \sqrt{\frac{1}{S_{II}}} S_{ij} \tag{15}$$

An alternative relation between symmetric rates of deformation and deviatoric stresses can be obtained from the definition of a viscous and incompressible fluid, i.e.

$$D_{ij} = \frac{1}{2\mu} S_{ij} \tag{16}$$

where $\mu > 0$ is the apparent viscosity.

From eqns (15) and (16), one can obtain the apparent viscosity of an isotropic, non-Newtonian fluid that models the flow of the granular solid in the form

$$\mu = \frac{\sqrt{S_{II}}}{\gamma [S_{II} - k^2 (p+c)^m (p-c)]} \tag{17}$$

Notice that the value of μ is a non-linear function of the second invariant of the deviatoric stress tensor, S_{II} and of the pressure p.

A more convenient expression for μ can be obtained in terms of D_{ij}. This can be achieved using the definition of S_{II} and D_{II} (the second invariant of the symmetric rate of deformation tensor)

$$S_{II} = \tfrac{1}{2} S_{ij} S_{ij} \quad D_{II} = \tfrac{1}{2} D_{ij} D_{ij} \tag{18}$$

Finally, from eqns (16)–(18) it is possible to obtain

$$\mu = \sqrt{\frac{2\gamma^{-1} \sqrt{D_{II}} + k^2 (p+c)^m (p-c)}{4 D_{II}}} \tag{19}$$

3.3. Experimental determination of constitutive parameters

The main interest in this work is to present a new constitutive model to model the flow of cohesive–frictional granular material and investigate its performance to simulate the discharge of silos and hoppers. A brief mention regarding how the parameters used in the model can be obtained experimentally is made in this section.

The most important information of the present constitutive model is summarized by the apparent viscosity [see eqn (19)]. For an adequate representation of a specific granular material, tests should be carried out to obtain experimental data about the parameters. There are two main classes of parameters that need evaluation: first, there are parameters which have been employed by other authors, such as friction angle and cohesion. Second, there are less common parameters, such as the exponent m (Gray and Stiles, 1990) and the fluidity (Diez and Godoy, 1992).

Eqn (9) can be solved for the exponent m

$$m = \frac{\ln \dfrac{S_{II}}{k^2(p-c)}}{\ln (p+c)} \tag{20}$$

With experimental values of cohesion and the frictional angle, one can plot $\sqrt{S_{II}}$ as a function of p when the material yields. To achieve this we follow Desai and Siriwardane (1984) and carry out cylindrical triaxial tests: conventional triaxial compression (CTC) and conventional triaxial extension (CTE) with the stress path having a positive slope; triaxial compression (TC), triaxial extension (TE) and simple shear (SS) with vertical stress paths. Finally, reduced triaxial compression (RTC) and reduced triaxial extension (RTE) with a stress path with a negative slope.

In some materials the value of m is not constant and varies with the relation between $\sqrt{S_{II}}$ and p. A mean value can be taken in such cases.

Notice that the exponent m is present because of a discrepancy between the critical state function and the Drucker–Prager function and for $m = 1$ the Drucker–Prager function is obtained. In other theories such as Cap models, the critical state function is not the same as in Drucker–Prager.

The fluidity parameter γ can be obtained by measurements of viscosity using a parallel-disk instrument, as explained by Bird et al. (1977). With the viscosity μ one can compute the value of γ from eqn (19) as

$$\gamma = \frac{2\sqrt{D_{II}}}{4\mu^2 D_{II} - k^2(p+c)^m(p-c)} \tag{21}$$

Another way to proceed according to Flavigny and Nova (1990) is by means of creep trixial test under constant values of S_{II} and p in order to obtain the viscosity.

Aubrey et al. (1985) mention that the fluidity is not constant due to films of absorbed water which modify the contacts between particles.

4. Finite element discretization

4.1. Formulation of viscous flow

The isothermal and incompressible flow of a viscous fluid in Eulerian coordinates is given by

$$\nabla \cdot \mathbf{T} + \mathbf{q} = \mathbf{0} \tag{22}$$

$\mathbf{T}$ is the Cauchy stress tensor and can be decomposed into a deviatoric and a spherical component as

$$\mathbf{T} = -p\mathbf{I} + \mathbf{S} \tag{23}$$

where $\mathbf{I}$ is the unit second-order tensor, p is the hydrostatic pressure

$$p = -\frac{T_{ii}}{3} \tag{24}$$

and $\mathbf{S}$ is the deviatoric tensor. The deviatoric stress tensor can be related to the deformation rate tensor by means of the apparent viscosity μ

$$S_{ij} = 2\mu D_{ij} \tag{25}$$

Substitution of eqn (19) into the last equation leads to

$$S_{ij} = 2\sqrt{\frac{2\gamma^{-1}\sqrt{D_{\mathrm{II}}} + k^2(p+c)^m(p-c)}{4D_{\mathrm{II}}}}D_{ij} \tag{26}$$

The mass forces per unit volume are $\mathbf{q}$. There are two contributions to $\mathbf{q}$: first the mass forces due to external actions ($\mathbf{b}$); and second, the effects due to the dynamic acceleration

$$\mathbf{q} = \mathbf{b} = \rho\left[\frac{\partial \mathbf{v}}{\partial t} + (\nabla \otimes \mathbf{v}^{\mathrm{t}})^{\mathrm{t}}\mathbf{v}\right] \tag{27}$$

where the symbol $\otimes$ indicates tensor product.

In the general case, the velocity vector is

$$\mathbf{v}^{\mathrm{t}} = (u_1, u_2, u_3) \tag{28}$$

However, attention is restricted in this case to plane and axisymmetric problems, for which $u_3 = 0$.

For stationary discharge of a silo, the time derivatives are zero, i.e. $[\partial(\,)/\partial t] = 0$. Finally, the velocity is assumed to be small, so that the convective acceleration can be neglected (see Schaffer, 1987)

$$\frac{\partial \mathbf{v}}{\partial t} + (\nabla \otimes \mathbf{v}^{\mathrm{t}})^{\mathrm{t}}\mathbf{v} = 0 \tag{29}$$

Finally, substitution of eqns (23), (26) and (29) into the equilibrium eqn (22) yields

$$2\frac{\partial}{\partial x_j}\left[\frac{\sqrt{2\gamma^{-1}\sqrt{D_{\mathrm{II}}} + k^2(p+c)^m(p-c)}}{4D_{\mathrm{II}}}D_{ij}\right] - \frac{\partial p}{\partial x_i} + \rho g_i = 0 \tag{30}$$

Notice that the above set of eqn (30) reduce to the Navier–Stokes equations whenever μ is constant. The difference is due to the dissipative term. In a viscous fluid the dissipation takes place due to collisions between molecules; however, in the flow with low velocities as in the discharge of grains, there is a sliding between particles. In the Navier–Stokes equations the dissipation is a function of the velocity and is independent of the pressure; however, in the present formulation the dissipation depends on the pressure and not on the velocity.

To obtain a more complete description of the flow, the continuity equation is required and in this case reduces to

$$\frac{\partial u_i}{\partial x_i} = 0 \tag{31}$$

Alternatively, one can write

$$D_{ii} = \nabla \cdot \mathbf{v}^{\mathrm{t}} = 0 \tag{32}$$

Finally, the boundary conditions of the problems are

$$u_i = w_i \tag{33}$$

$$T_{ij} n_j = h_i \tag{34}$$

- Eqn (33) is a kinematic boundary condition appropriate for solid boundaries and symmetry conditions. This is the only boundary condition employed in the computations of the present work.
- For a rigid boundary the condition of no penetration is satisfied; furthermore, the condition of no sliding is considered in the present computations. To model the grain–wall friction a thin layer of finite elements has been employed next to the wall. Experimental values of cohesion and friction for grain–wall interface should be employed on those elements. This is an accurate and economical technique which has been employed previously in the context of metal forming processes and by the authors for the discharge of silos (Diez and Godoy, 1992; Elaskar et al., 1996).
- For conditions of symmetry, the transverse component of velocity should be zero. This is imposed at the center of a silo when there are symmetric conditions of geometry, material and flow.
- For the transient discharge of silos, the mechanical boundary condition of eqn (34) is a possible way to consider the frictional effects that occur between the grains and the walls (see Haussler and Eibl, 1984). If a model with Newtonian friction between grain and wall is employed, then a non-linearity is introduced into the formulation on the boundary condition and it is necessary to use eqn (34).

For the finite element discretization of the model it is convenient to employ the following matrix notation

$$D_{ii} = \mathbf{m}^{\mathrm{t}} \mathbf{D} = 0 \tag{35}$$

where $\mathbf{m}^{\mathrm{t}} = (1, 1, 0)$ for planar problems; and $\mathbf{m}^{\mathrm{t}} = (1, 1, 0, 1)$ for axisymmetric problems.

The symmetric rate of deformation tensor is

$$\mathbf{D} = \mathbf{L}\mathbf{v} \tag{36}$$

where, for plane problems

$$\mathbf{L} = \begin{bmatrix} \dfrac{\partial}{\partial x_1} & 0 \\ 0 & \dfrac{\partial}{\partial x_2} \\ \dfrac{\partial}{\partial x_2} & \dfrac{\partial}{\partial x_1} \end{bmatrix} \tag{37}$$

$$\mathbf{D}^{\mathrm{t}} = (D_{11}, D_{22}, 2D_{12}) \tag{38}$$

while for axisymmetric problems

$$\mathrm{L} = \begin{bmatrix} \dfrac{\partial}{\partial x_1} & 0 \\ 0 & \dfrac{\partial}{\partial x_2} \\ \dfrac{\partial}{\partial x_2} & \dfrac{\partial}{\partial x_1} \\ \dfrac{1}{x_1} & 0 \end{bmatrix} \tag{39}$$

$$\mathbf{D}^{\mathrm{t}} = (D_{11}, D_{22}, 2D_{12}, D_{33}) \tag{40}$$

For an incompressible, viscous and isotropic fluid, the constitutive equations are (Zienkiewicz and Taylor, 1991)

$$\mathbf{S}^{*} = \boldsymbol{\mu}\mathbf{E}^{\mathrm{s}}\mathbf{D} \tag{41}$$

Matrix $\mathbf{E}^{\mathrm{s}}$ is diagonal. For plane problems one has

$$\mathbf{E}^{\mathrm{s}} = \begin{bmatrix} 2 & 0 & 0 \\ 0 & 2 & 0 \\ 0 & 0 & 1 \end{bmatrix} \tag{42}$$

while for axisymmetric problems

$$\mathbf{E}^{\mathrm{s}} = \begin{bmatrix} 2 & 0 & 0 & 0 \\ 0 & 2 & 0 & 0 \\ 0 & 0 & 1 & 0 \\ 0 & 0 & 0 & 2 \end{bmatrix} \tag{43}$$

4.2. Integral formulation

The weak formulation of the equilibrium problem in eqn (22) yields the virtual power condition

$$\int_{\Omega} \delta D_{ij} T_{ij} \, \mathrm{d}\Omega = \int_{\Omega} \delta u_i b_i \, \mathrm{d}\Omega + \int_{\Gamma} \delta u_i t_i \, \mathrm{d}C \tag{44}$$

The forces t_i are applied on the boundary Γ of the body, while the volume forces b_i act on the volume Ω. The symbol δu_i indicates the virtual variation of u_i.

The continuity condition states that any virtual variation of the pressure, δp, does not produce work (see, for example, Hughes, 1987).

$$\int_{\Omega} \delta p D_{ii} \, \mathrm{d}\Omega = 0 \tag{45}$$

A penalty function is next introduced, so that the pressure is not a primary variable of the formulation. Volume changes in the incompressible fluid are written as

$$D_{ii} = -\frac{p}{\alpha} \approx 0 \tag{46}$$

where α is a penalty parameter, which is a finite but large value, to ensure the incompressibility condition in approximate form.

Then, eqn (44) can also be written as

$$\int_\Omega \delta D_{ij} 2\mu D_{ij} \, d\Omega + \alpha \int_\Omega \delta D_{ii} D_{ii} \, d\Omega = \int_\Omega \delta u_i b_i \, d\Omega + \int_C \delta u_i t_i \, dC \tag{47}$$

4.3. Discretization

The discretization of the velocity field is carried out in this work by finite elements, leading to

$$\mathbf{v} = \mathbf{N}\mathbf{a}^e \tag{48}$$

where matrix $\mathbf{N}$ contains the shape functions of a given element Ω^e and the nodal values of velocity are

$$\mathbf{a}^e = \left(u_1^1, u_1^2, \ldots, u_1^N, u_1^N\right) \tag{49}$$

Lagrangian quadrilateral elements with nine nodes are used in this work. The formulation of such elements is rather standard and may be found in texts on finite elements such as Zienkiewicz and Taylor (1991). The final form of the assembled system is

$$\left[\mathbf{K}^s(\mathbf{a}) + \alpha \mathbf{K}^v)\right]\mathbf{a} = \mathbf{f} \tag{50}$$

where $\mathbf{K}^v$ are the volumetric contributions and $\mathbf{K}^s$ are the deviatoric components; $\mathbf{f}$ is the global load vector and $\mathbf{a}$ is the global velocity vector. This is a non-linear system due to the constitutive model employed.

4.4. Numerical integration

In eqn (50) one can verify that for large values of α (the penalty parameter) then

$$\mathbf{K}^v\mathbf{a} \approx \frac{\mathbf{f}}{\alpha} \to 0 \tag{51}$$

Thus, to obtain a non-trivial solution it is necessary to impose a condition of singularity on $\mathbf{K}^v$. This has been noticed by many authors (see, for example, Hughes et al., 1979) and reduced integration has been used to model the singularities in $\mathbf{K}^v$, while standard integration is imposed upon $\mathbf{K}^s$.

The viscosity μ is evaluated at four integration points on each element, according to the reduced integration rule adopted. Several ways can be followed to have μ at other points and a constant value of μ has been adopted in this work as the average

$$\mu^e = \tfrac{1}{4}\left(\mu_1^e + \mu_2^e + \mu_3^e + \mu_4^e\right) \tag{52}$$

The penalty parameter varies from one element to another according to the value of μ^e, in the form

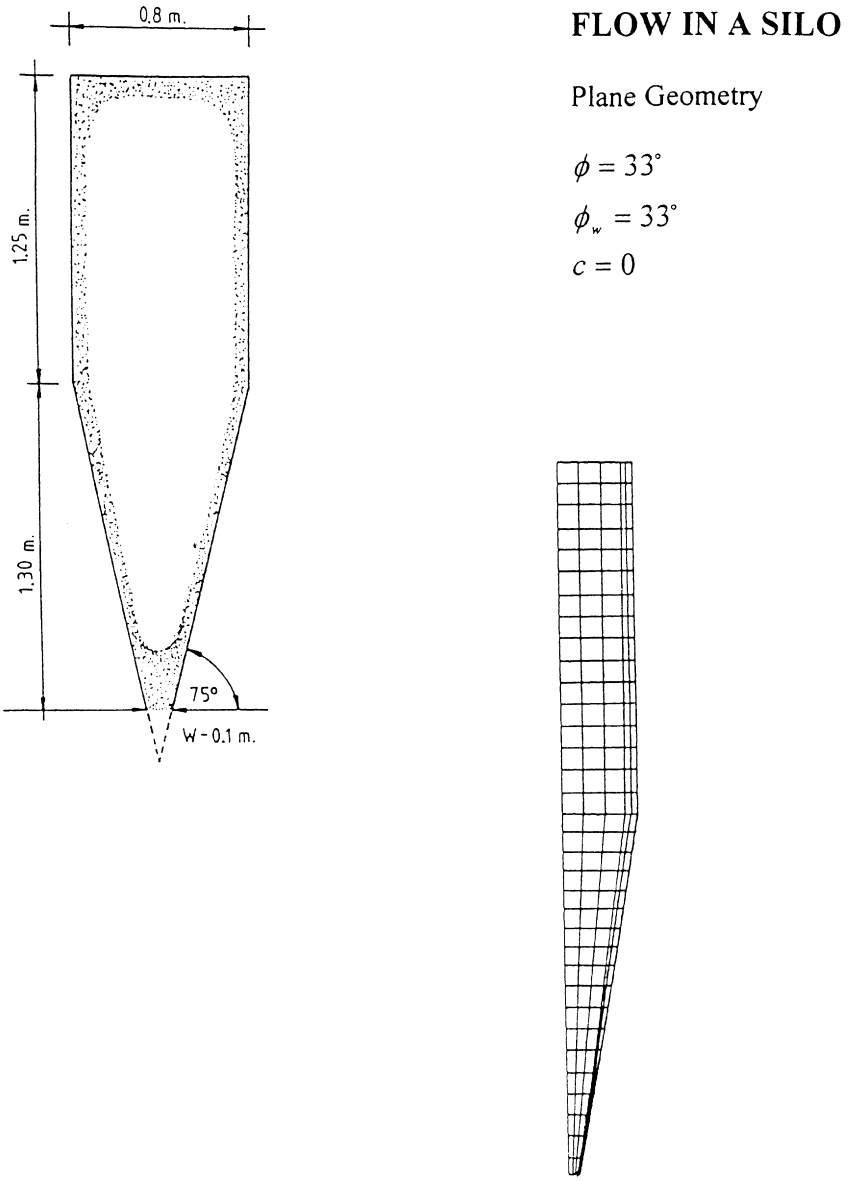

Fig. 3. Geometric description of the plane silo studied by Kmita.

$$\alpha^e = \varsigma \mu^e \tag{53}$$

where ς takes values between 10^4–10^{10}. This option has been implemented in the present code because the convergence characteristics are improved with respect to other options considered.

4.5. Solution of non-linear system

Direct iteration has been employed to solve the non-linear system of equations. Notice that matrix $\mathbf{K}^s$

depends on the viscosity μ, while μ depends on D_{II} and p. Direct integration has been employed in the present context for example by Oñate (1986) for metal forming problems and will not be described here.

5. Comparison with experimental results

Two sets of experimental results have been used to compare with our computational simulation. The first is a silo, Fig. 3, while the second is a hopper shown in Fig. 4. It should be mentioned that it is difficult to find experiments published in the literature with the appropriate parameters identified so as to check numerical models.

The silo is a plane problem, while the hopper is axisymmetric and both have been discretized using 130 Lagrangian elements. The boundaries are assumed to have zero velocity (no slip) in contact with the

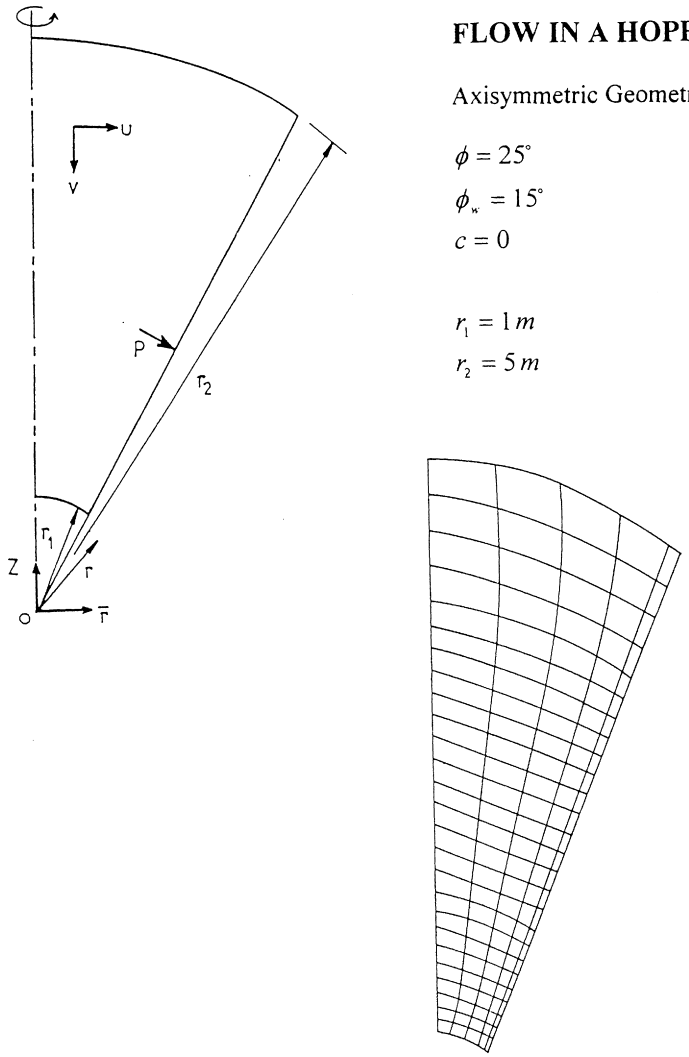

Fig. 4. Geometric description of the axisymmetric hopper.

walls of the structure. However, a thin layer of finite elements is introduced in contact to the wall to simulate the frictional properties between granular solid and wall. Initial conditions are not specified because the problem is solved as steady-state. The only external action present in this problem is gravity.

5.1. Plane silo

Kmita (1991) tested the flow in a silo of 2.55 m in height filled with rinsed grit with $c = 0$, $\phi = 33^\circ$ and the angle of friction between the granular material and the wall was $\phi = 33^\circ$. Here we adopt a discontinuity surface with $m = 0.65$ and for the viscoplastic flow we used $\gamma = 1$ 1/kPa s and $\rho = 1623$ kg/m^3. The iterative procedure starts with a constant value of $\mu_0 = 150$ kPa s throughout the mesh of 130 elements and convergence is achieved with a norm $\varepsilon = 0.01$. The angles of friction ϕ, ϕ_w and the density ρ are taken from Kmita (1991). The exponent m and the fluidity γ should be obtained from the experiment for specific granular materials, but in this work we have representative values and explore the sensitivity of the solution as they change.

The results presented by Kmita (1991) are restricted to pressures on the wall of the silo and these are compared with our results in Fig. 5.

For this complex problem, the numerical results show qualitative agreement with the experiment and good numerical correlation. The pressure distribution along the lower part of the silo, for which there is experimental data, shows the same trend and the peak pressure at the junction between the two geometries of the silo is estimated well by the computations.

The distribution of viscosities at the steady state is shown in Fig. 6. Close to the outlet of the silo one

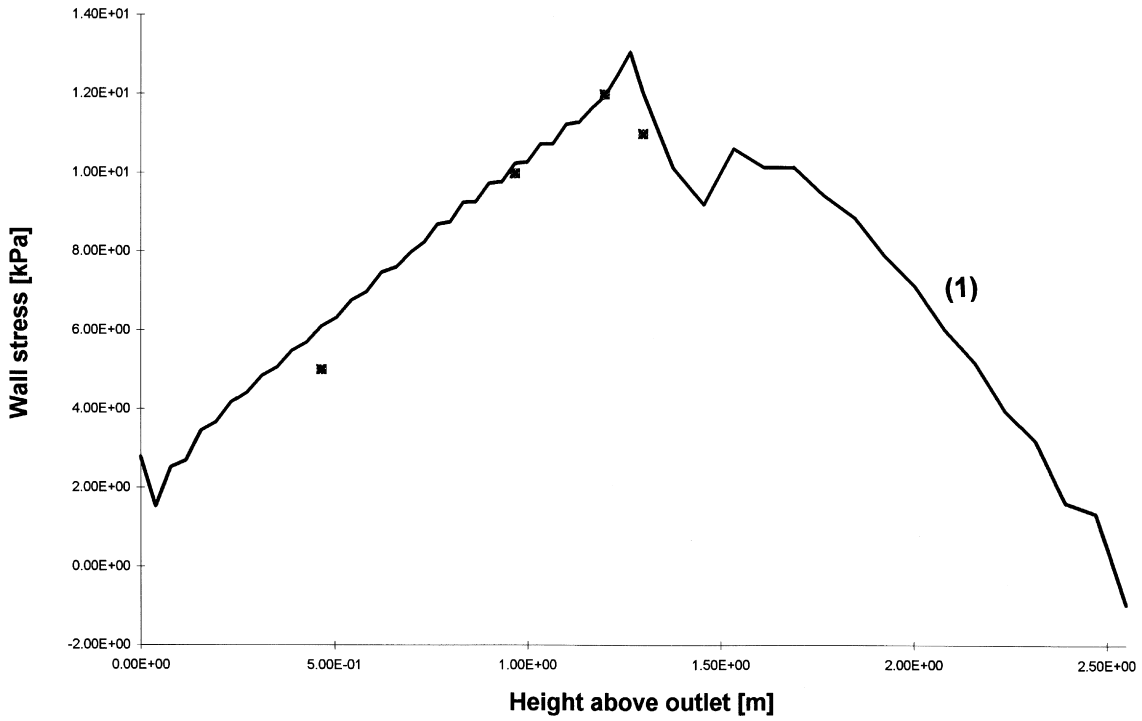

Fig. 5. Comparison of present result with experimental values by Kmita. (1) Present result, ■ values of Kmita.

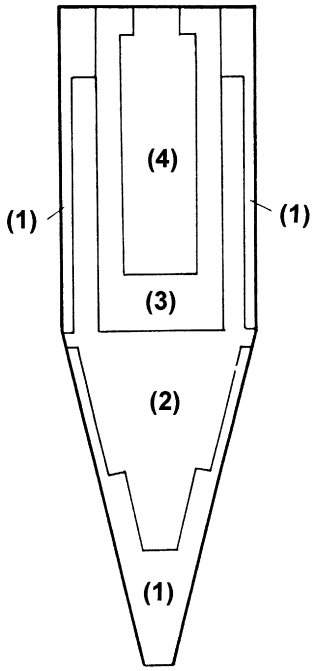

Fig. 6. Distribution of viscosities inside the plane silo. (1) 0.01 kPa s $\leqslant \mu <$ 10 kPa s, (2) 10 kPa s $\leqslant \mu <$ 100 kPa s, (3) 100 kPa s $\leqslant \mu <$ 1000 kPa s, (4) $\mu \geqslant$ 1000 kPa s.

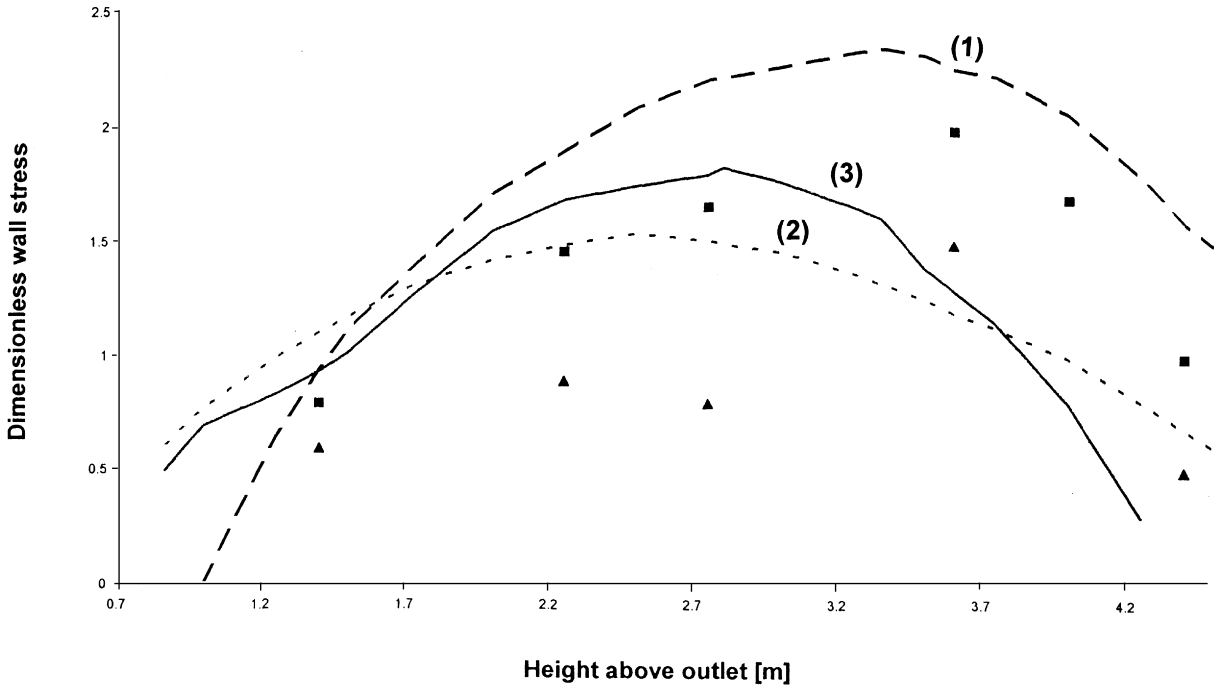

Fig. 7. Comparison of present results with other experimental and analytic results. (1) Theory of Nguyen et al. (2) theory of Walker and Blanchard, (3) present result, ■ Walker upper bound, ▲ Walker lower bound.

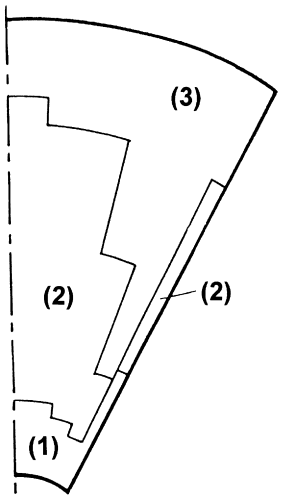

Fig. 8. Distribution of viscosities inside of the axisymmetric hopper. (1) 0.01 kPa s $\leqslant \mu <$ 10 kPa s, (2) 10 kPa s $\leqslant \mu <$ 100 kPa s, (3) 100 kPa s $\leqslant \mu <$ 1000 kPa s.

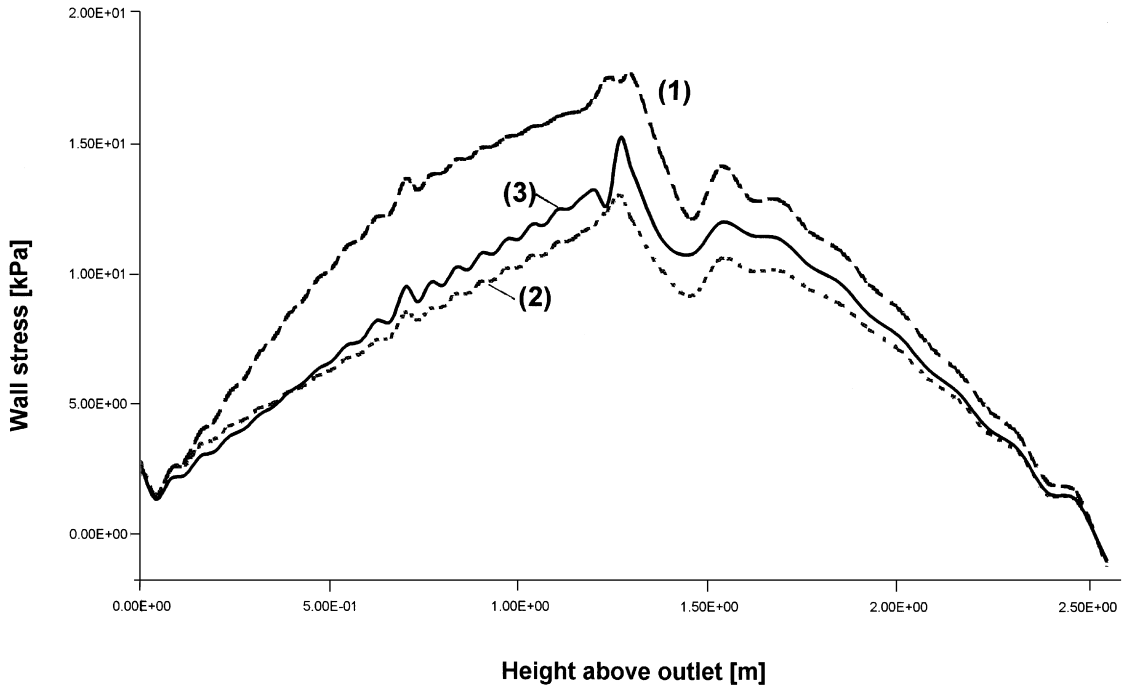

Fig. 9. Silo. Influence of the fluditiy parameter on the wall stress. (1) $\gamma = 0.1$ 1/kPa s, (2) $\gamma = 1$ 1/kPa s, (3) $\gamma = 10$ 1/kPa s.

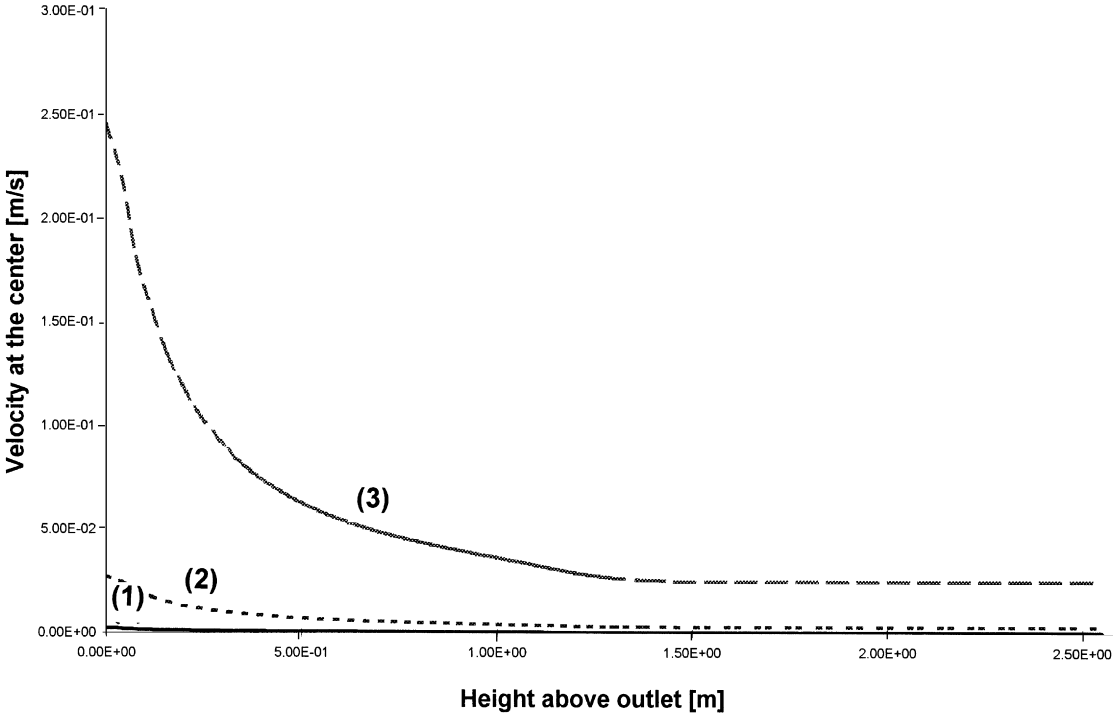

Fig. 10. Silo. Influence of the fluidity parameter on the center velocity. (1) $\gamma = 0.1$ 1/kPa s, (2) $\gamma = 1$ 1/kPa s, (3) $\gamma = 10$ 1/kPa s.

finds small values of viscosities and these are increased near to the top of the silo. In general terms, the viscosity μ increases from bottom to top and from the walls to the center of a vertical silo under gravity flow.

5.2. Axisymmetric hopper

Our second example to test the present model is an axisymmetric hopper studied by Walker and Blanchard (1967) and Nguyen et al. (1979) using analytical models and by Walker and Blanchard (1967) by means of experiments. The geometry is shown in Fig. 4, with zero cohesion, an angle of friction of 25° and a grain–wall friction angle of 15°.

The mesh employed for the hopper has 130 elements. Data for this case is as follows: $\phi = 25°$, $\phi_w = 15°$, $m = 1.5$, $\gamma = 1$ 1/kPa s, $\varepsilon = 0.01$, $\rho = 150$ kg/m^3, and $\mu_0 = 150$ kPa s, values of friction angles and density were taken from Walker and Blanchard (1967) and Nguyen et al. (1979).

Results of stresses on the wall are plotted in Fig. 7 for different elevations. We have also plotted what are called the upper bound and lower bound experimental results in the paper of Walker and Blanchard (1967). The present model has good agreement at the lower part of the hopper, i.e. up to approximately 3 m in height. At the top of the hopper, the present model yields values close to the lower bound. There is also a good estimate of the maximum load on the wall. Independent analytical results are also shown in Fig. 7.

An interesting point is to investigate how the apparent viscosity μ changes inside the bulk solid at the steady state. Results are shown in Fig. 8, with low values of μ at the lower part of the hopper and close

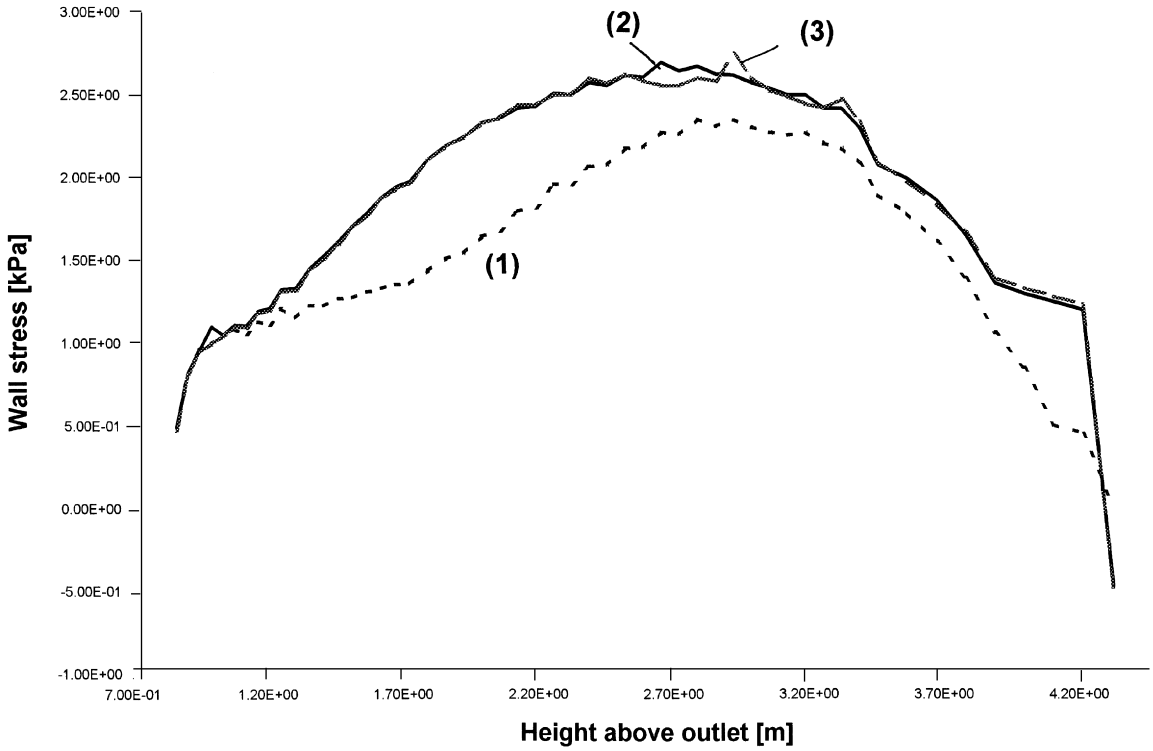

Fig. 11. Hopper. Influence of the fluidity parameter on the wall stress. (1) $\gamma = 0.1$ 1/kPa s, (2) $\gamma = 1$ 1/kPa s, (3) $\gamma = 10$ 1/kPa s.

to the walls (0.01 kPa s $\leqslant \mu \leqslant$ 10 kPa s), where the maximum velocities occur. Large values of μ are computed at the top of the hopper ($\mu > 100$ kPa s).

6. Numerical results

The sensitivity of the numerical solution with respect to changes in the internal parameters of the model is investigated in this section. There are some physical parameters, such as the fluidity parameter γ, the exponent m, the angle ϕ, the cohesion c, etc., for which it would be important to understand how they influence the response. A second group of parameters is related to the technique of the solution adopted in this work, including the penalty parameter α and the initial viscosity μ_0.

In the steady-state solution, the apparent viscosity μ is a variable in terms of the location inside the flowing grain. To start the iterative process we assume an initial viscosity and this is redefined during the iterations until convergence is reached. With the converged values of pressure and velocity, the viscosity also reaches convergence.

In the studies that follow we have solved the problems using a constant value of the initial vicosity, μ_0, throughout the finite element mesh.

Two cases are considered to carry out the parametric studies: the silo and the hopper discussed in the previous section. The purpose of the studies that follow is to investigate how the choice of a parameter

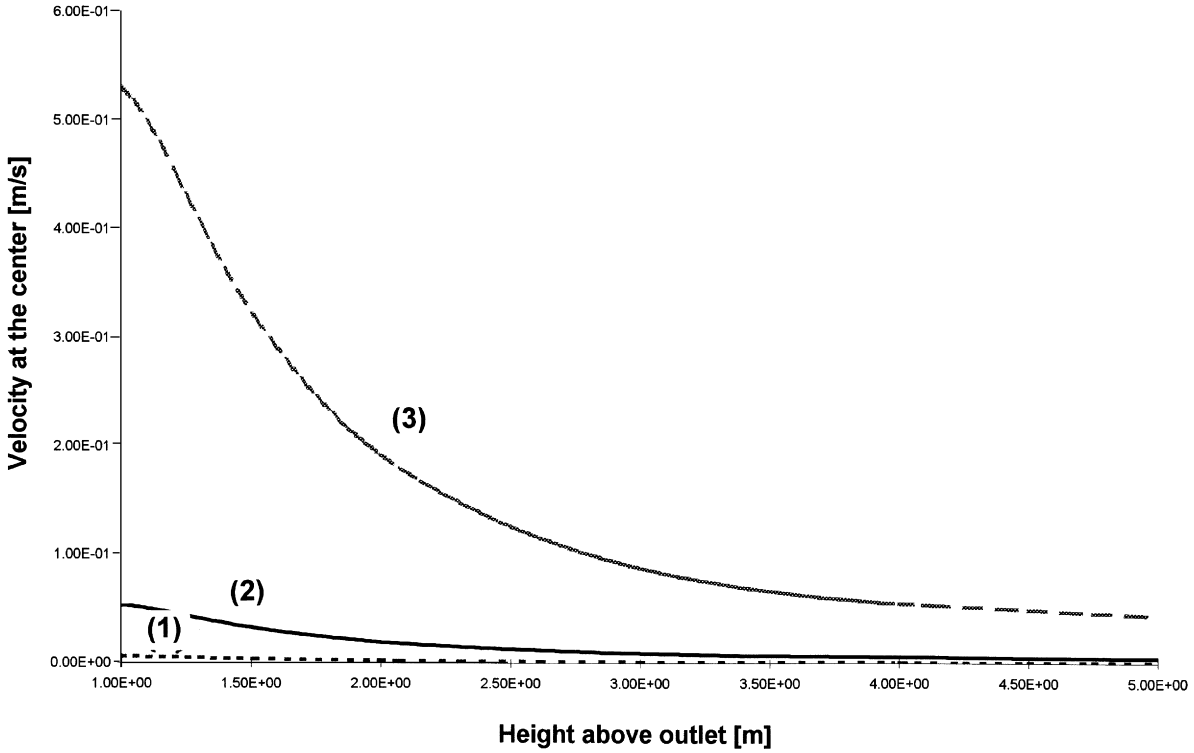

Fig. 12. Hopper. Influence of the fluidity parameter on the center velocity. (1) $\gamma = 0.1$ 1/kPa s, (2) $\gamma = 1$ 1/kPa s, (3) $\gamma = 10$ 1/kPa s.

influences the solution and as such this indicates what parameters should be determined experimentally with better accuracy.

6.1. Influence of the fluidity parameter

6.1.1. Plane silo

For the silo considered and with a constitutive model with $m = 0.65$, we have computed results of pressure and velocities for different values of the fluidity parameter. The values assumed in Figs. 9 and 10 are $\gamma = 0.1$, 1 and 10 1/kPa s. The initial viscosity was taken as constant, with $\mu_0 = 150$ kPa s.

The pressures on the wall are shown in Fig. 9 and display the same pattern even though there are significant changes in γ. There is an increase from 13–15 kPa in the maximum pressure, as γ is increased from 1–10 1/kPa s.

The velocity at the center is shown in Fig. 10 and are seen to increase with the fluidity γ. For $\gamma = 0.01$ 1/kPa s the velocity is very small.

As γ increases, the number of iterations required to obtain convergence also increases. For example, with $\gamma = 0.1$ 1/kPa s the number of required iterations was 21; with $\gamma = 1$ 1/kPa s the number of required iterations was 27; while 35 iterations were necessary to obtain convergence for $\gamma = 10$ 1/kPa s.

6.1.2. Axisymmetric hopper

A similar investigation on the influence of γ was carried out for the hopper and the results are

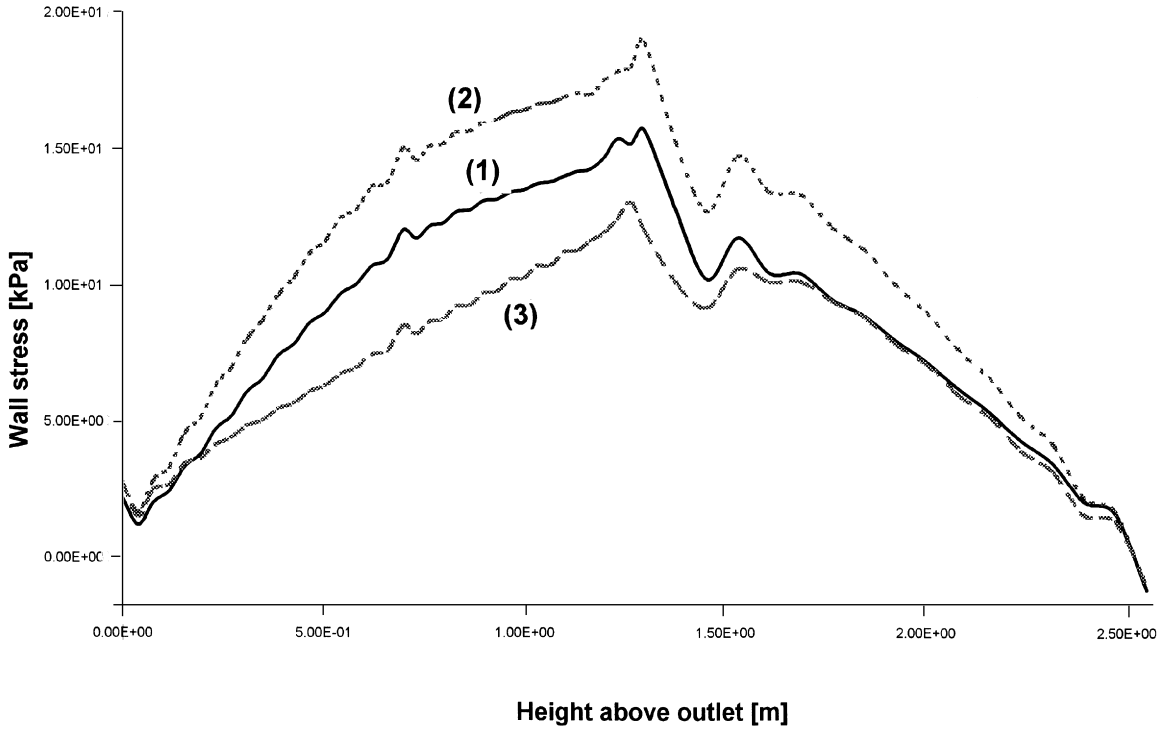

Fig. 13. Silo. Wall stress sensitivity with respect to changes in the exponent m on the discontinuity surface. (1) $m = 0.5$, (2) $m = 0.6$, (3) $m = 0.65$.

summarized in Figs. 11 and 12. The pressures are almost the same for $\gamma = 1$ and 10 1/kPa s, but for $\gamma = 0.1$ 1/kPa s there are smaller values of pressure on the walls.

The velocity at the center of the hopper increases with γ, as in the case of the silo.

The number of iterations necessary to obtain convergence of the solution was as follows: $\gamma = 0.1$, 1 and 10 1/kPa s for 22, 28 and 30 iterations, respectively.

Notice that both the silo and the hopper displayed similar flow behavior as a function of the fluidity parameter γ, even though they included different bulk material and geometries. The overall conclusion of this parametric study is that it is necessary to carry out experimental studies to evaluate γ for cereals; but it seems that for practical cases ($\gamma \geqslant 1$ 1/kPa s) the pressure are not very sensitive to errors in the evaluation of γ. The velocity of the particles during discharge, on the other hand, are highly dependent on fluidity.

6.2. Sensitivity with respect to changes in the exponent m of the discontinuity surface

The value of the exponent m in eqn (9) characterizes the shape of the discontinuity surface employed as seen in Fig. 2.

6.2.1. Plane silo

Parametric studies were conducted on the plane silo problem to observe the influence of m on the

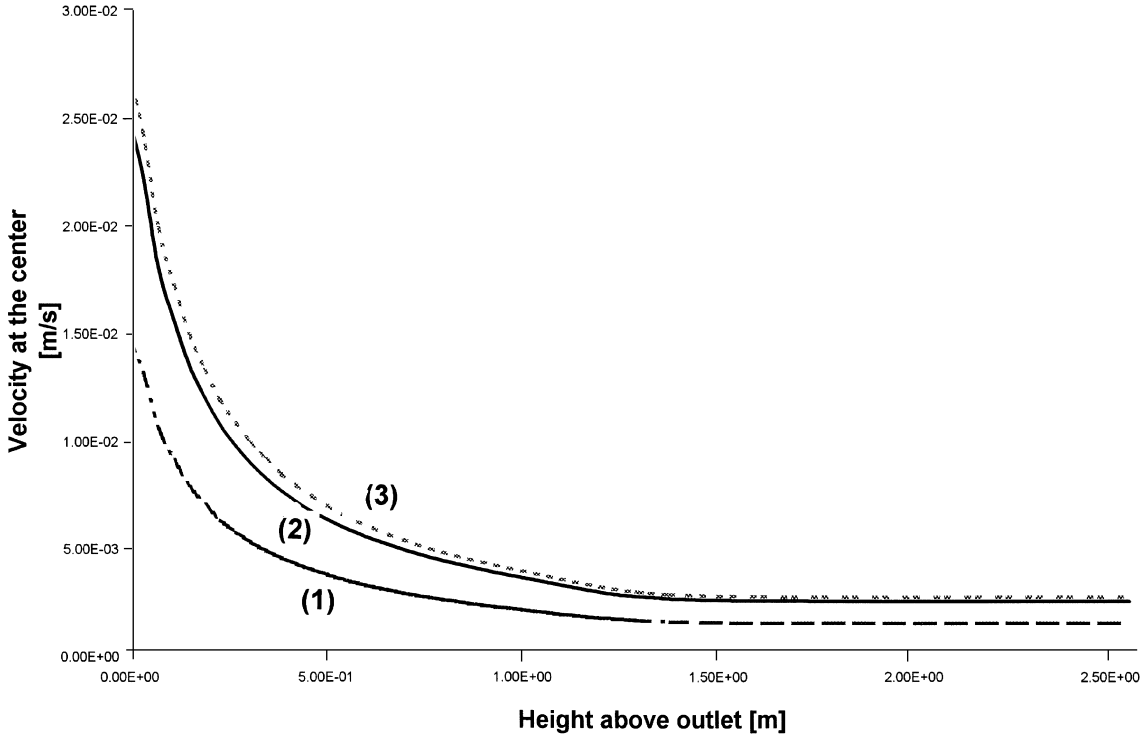

Fig. 14. Center velocity sensitivity with respect to changes in the exponent m on the discontinuity surface. (1) $m = 0.5$, (2) $m = 0.6$, (3) $m = 0.65$.

velocity and pressure, using the values $m = 0.5$, 0.6, 0.65, 0.7 and 1.3. The other parameters of the constitutive equation were $\gamma = 1$ 1/kPa s, with $\mu_0 = 150$ kPa s.

The pressure does not have a monotonic change with m. The maximum pressures were obtained in Fig. 13 with $m = 0.6$, for which it was necessary to iterate 22 times. For $m = 0.65$, on the other hand, 27 iterations were required; for $m = 0.5$ convergence required 14 iterations; and no convergence was obtained with $m > 0.65$.

The values of velocity are shown in Fig. 14, with the lowest values occurring for $m = 0.5$ and the maximum for $m = 0.65$. The best approximation to the experimental results was shown to occur for $m = 0.65$.

6.2.2. Axisymmetric hopper

A study on the influence of m was also done for the hopper problem, using values of 0.65, 1.0, 1.5, 1.65, 1.7 and 1.75. The results are presented in Figs. 15 and 16 and reflect the response to different material properties.

Both the pressures on the wall and the velocity increase with the value of m are considered.

All four curves considered in Fig. 15 fall within the range of experimental results; however, a better approximation is obtained with $m = 1.5$ and $m = 1.65$. Lack of convergence of the iterative process was found for $m \geqslant 1.7$.

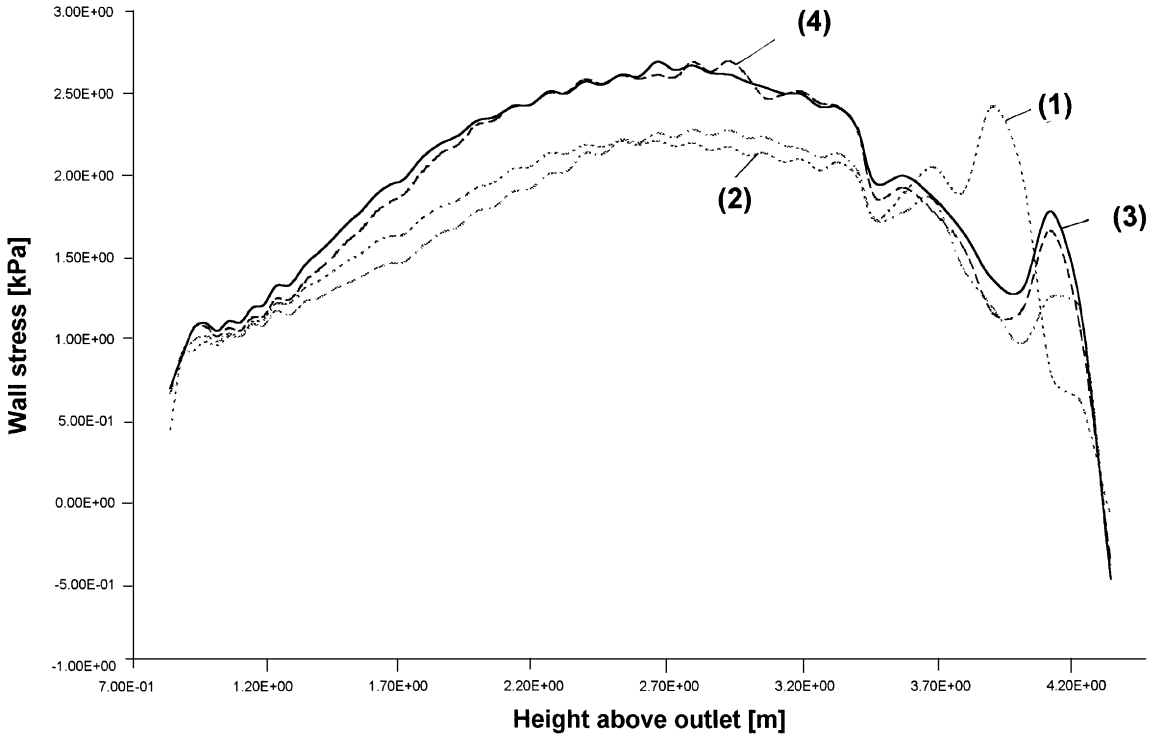

Fig. 15. Hopper. Wall stress sensitivity with respect to changes in the exponent m on the discontinuity surface. (1) $m = 0.65$, (2) $m = 1$, (3) $m = 1.5$, (4) $m = 1.65$

Notice that one cannot identify appropriate values of m from the present parametric studies; in any case they should be obtained experimentally as indicated by Gray and Stiles (1991). What the present studies highlight is the variability of pressures with m, especially for lower values of the exponent.

6.3. Influence of the initial viscosity

The initial viscosity μ_0 is introduced at the beginning of the iterative process, but the actual value chosen to start the analysis has an influence on the final results.

6.3.1. Plane silo

For the silo problem we have performed the analysis using $\mu_0 = 25$, 50 and 150 kPa s and the results are presented in Fig. 17 (pressures) and Fig. 18 (velocities). The pressure profile obtained is the same in all cases, with some differences between the lowest values ($\mu_0 = 25$ kPa s) and higher values ($\mu_0 = 50$ or 150 kPa s). The same trend is shown in Fig. 18 for velocities.

The number of iterations necessary to obtain convergence of the solution with $\varepsilon = 0.01$ is as follows: $\mu_0 = 25$, 50 and 150 kPa s with 25, 26 and 27 iterations, respectively.

6.3.2. Axisymmetric hopper

Three values of μ_0 were considered in this case: $\mu_0 = 50$, 100 and 150 kPa s.

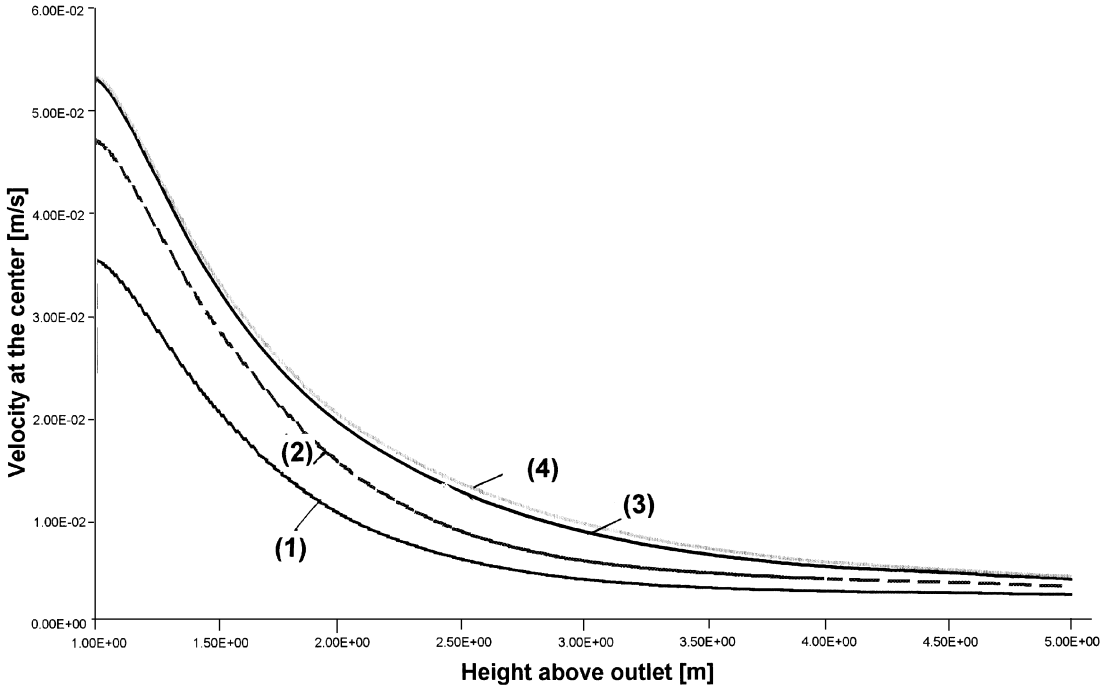

Fig. 16. Hopper. Center velocity sensitivity with respect to changes in the exponent m on the discontinuity surface. (1) $m = 0.65$, (2) $m = 1$, (3) $m = 1.5$, (4) $m = 1.65$.

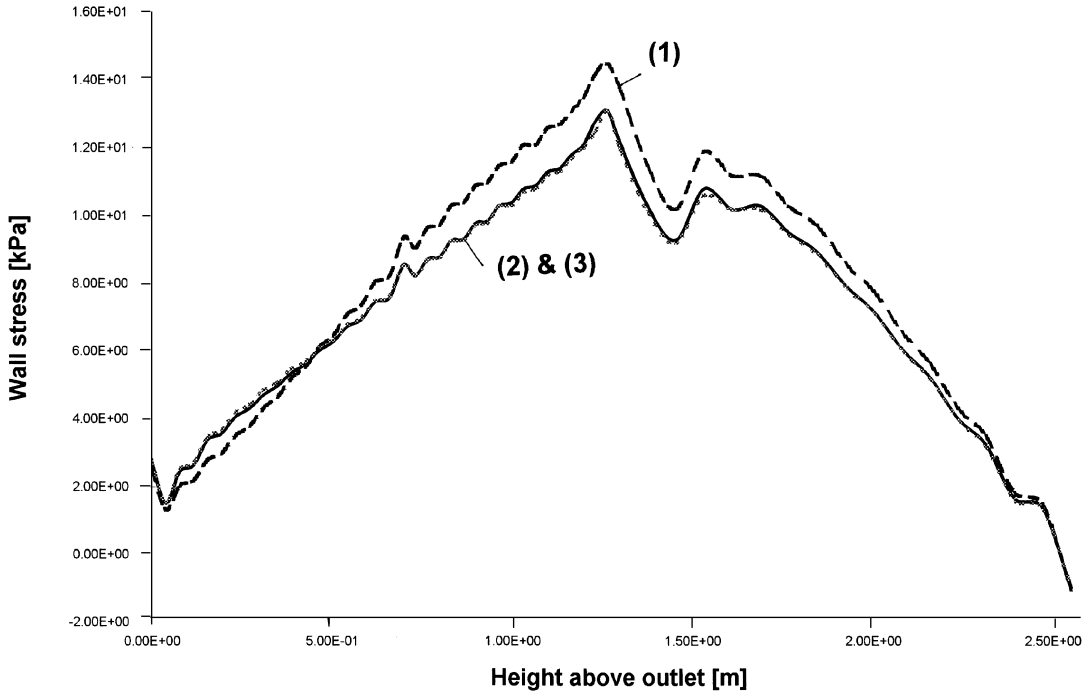

Fig. 17. Silo. Influence of the initial viscosity on the wall stress. (1) $\mu_0 = 25$ kPa s, (2) $\mu_0 = 50$ kPa s, (3) $\mu_0 = 150$ kPa s.

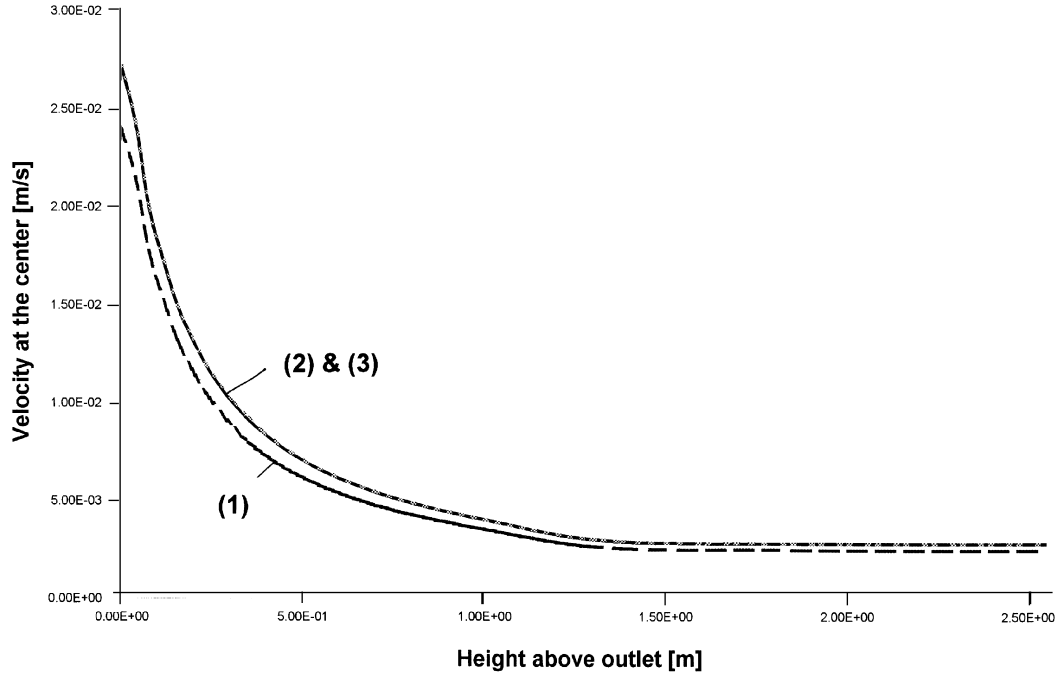

Fig. 18. Silo. Influence of the initial viscosity on the center velocity. (1) $\mu_0 = 25$ kPa s, (2) $\mu_0 = 50$ kPa s, (3) $\mu_0 = 150$ kPa s.

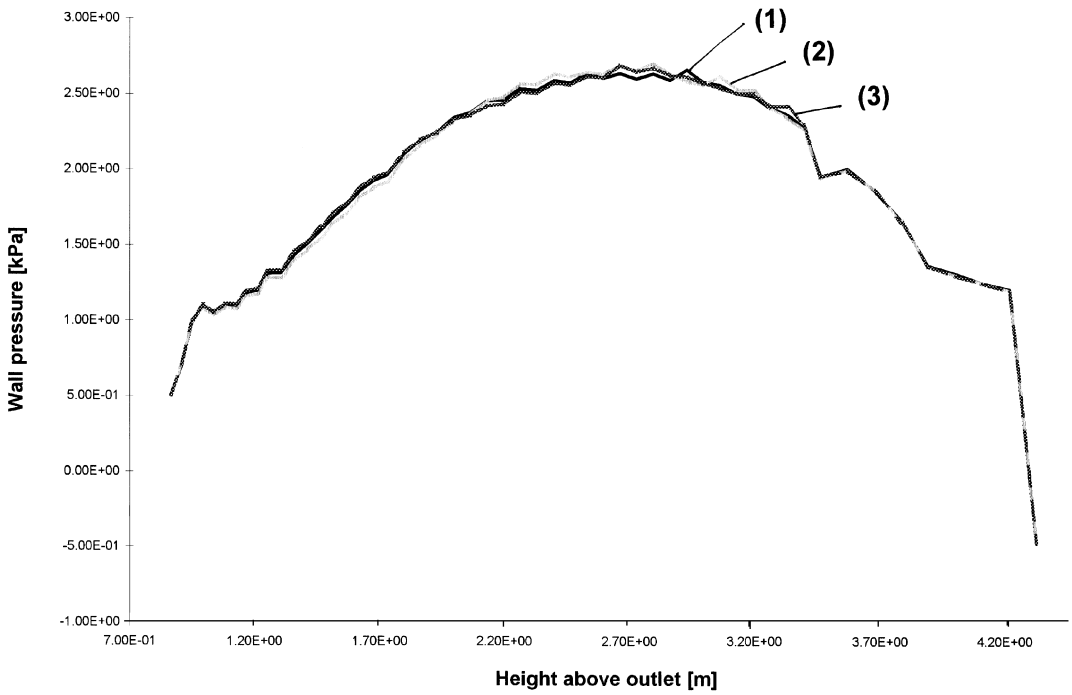

Fig. 19. Hopper. Influence of the initial viscosity on the wall stress. (1) $\mu_0 = 50$ kPa s, (2) $\mu_0 = 100$ kPa s, (3) $\mu_0 = 150$ kPa s.

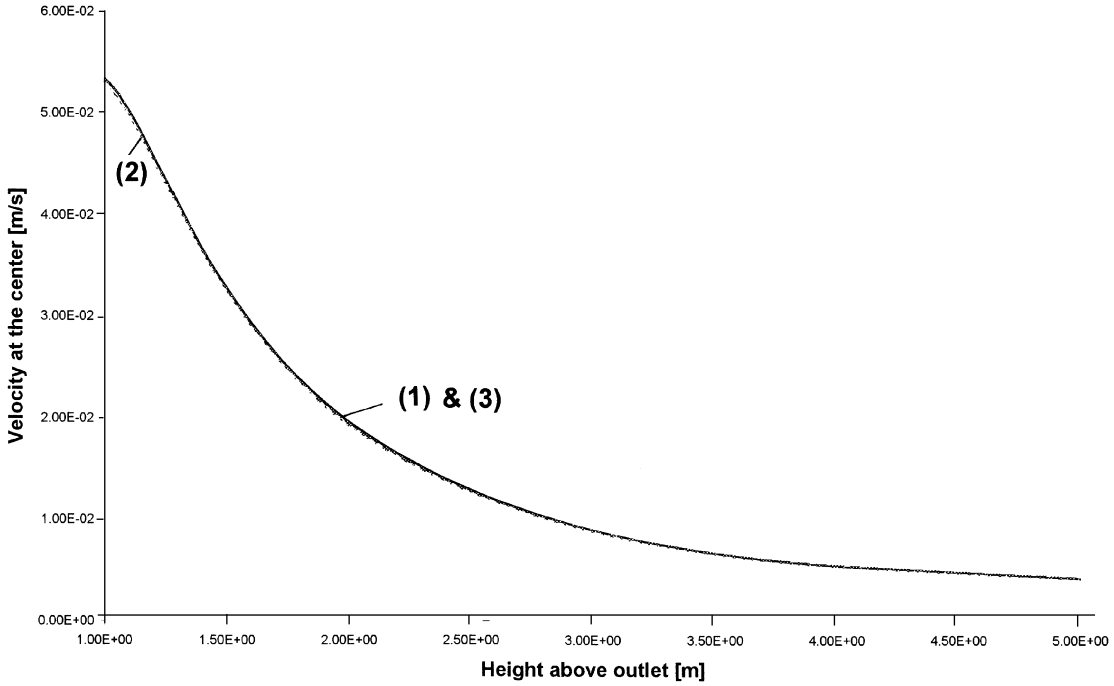

Fig. 20. Hopper. Influence of the initial viscosity on the center velocity. (1) $\mu_0 = 50$ kPa s, (2) $\mu_0 = 100$ kPa s, (3) $\mu_0 = 150$ kPa s.

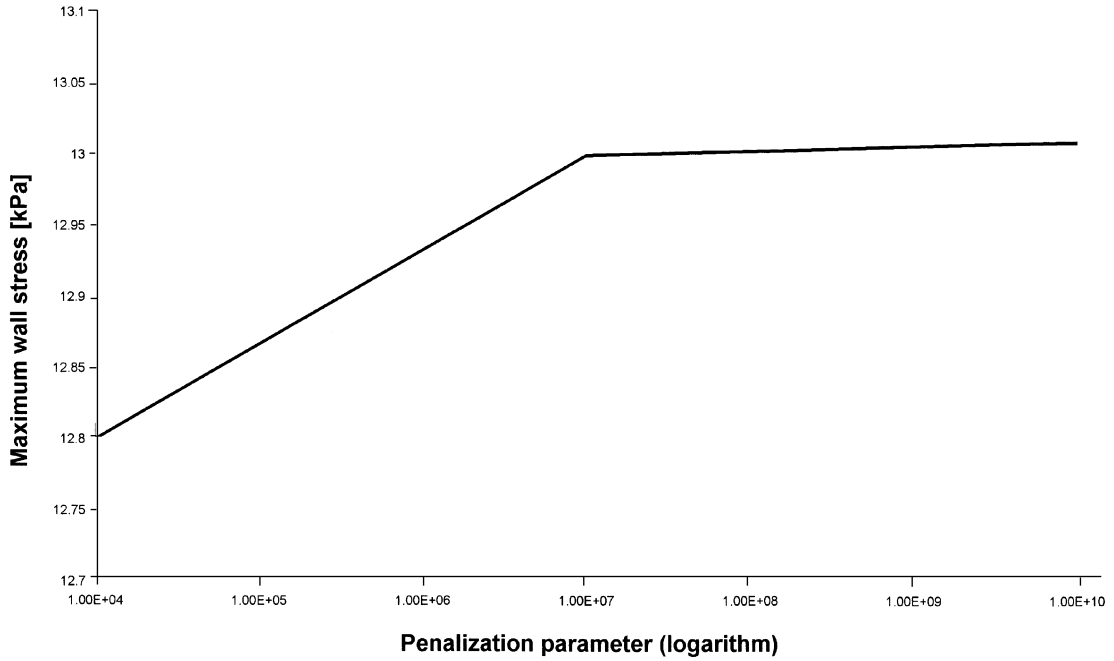

Fig. 21. Silo. Influence of the penalty parameter α on the maximum wall stress.

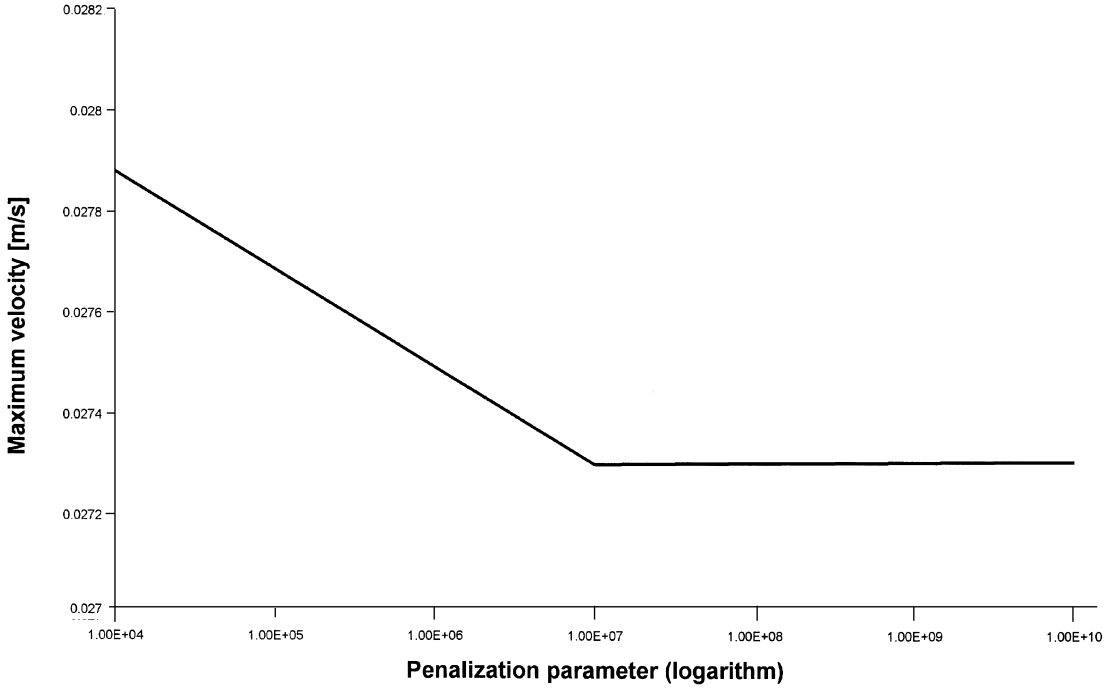

Fig. 22. Silo. Influence of the penalty parameter α on the outlet velocity.

The initial viscosity μ_0 has a negligible influence on the values of pressures and velocities as reflected by Figs. 19 and 20.

6.4. Influence of the penalty parameter α

In our final study, the actual value of the penalty parameter α is investigated for the silo of Fig. 5. The values of α considered were $\alpha = 10^4$, 10^7 and 10^{10}. The results of Figs 21 and 22 show that the solution stabilizes for large values of $\alpha \geqslant 10^7$. Similar conclusions were obtained for a number of other problems, so that α is recommended to be set to 10^7 or larger.

7. Discussion

The presentation of previous sections concentrated on the simulation of pressures on the walls of silos and hoppers during a stationary discharge. Furthermore, sensitivity studies were performed to understand the influence of different constitutive parameters on the results. In this section a few remarks are made regarding the application of the model to a new situation for a given material stored inside the silo:

- The geometry of the silo should be available.
- A finite element mesh should be built, including a thin layer of elements close to the boundaries to model the wall–grain friction. The angle of friction between the wall and the grain should be known or estimated.
- The constitutive parameters of the material should be specified, including cohesion, friction, fluidity and the exponent m. There is a large literature on the evaluation of cohesion and friction; however,

fluidity should be evaluated using the techniques mentioned in Section 3.3.

- For values of fluidity larger than 1 1/kPa s, the present numerical results show that the pressures on the walls are not affected by fluidity. Of course, this observation is based on a limited number of cases studied, however, for different silo geometries and material properties, the loads on the walls are not affected by fluidity larger than $\gamma \geqslant 1$ 1/kPa s.
- The exponent m required by the present model should be evaluated experimentally as indicated in Section 3.3. The numerical results showed that the best fitting to experimental results was obtained with the largest value of m for which convergence was achieved.
- A penalty parameter $\alpha \geqslant 10^7$ was found to be adequate for all purposes, including velocities and pressures and is recommended. Such values are also recommended in the literature for viscous and incompressible flows (Hughes, 1987).
- Finally, the initial viscosity μ_0 should be specified to start the computations. Studies of sensitivity of the solution for different choices of μ_0 in hoppers show that it does not affect the results in the present model, so that a value of $\mu_0 = 150$ kPa s may be employed as a starting guess in these cases. The iterative process evolves from the initial guess to the converged result.

8. Conclusions

The main conclusions drawn from the present constitutive model and the numerical studies may be summarized as follows:

The constitutive equation presented in this work can model the main features of the steady mass-flow in silos and hoppers. It also seems that the hypothesis of flow under critical conditions (incompressible behavior) is adequate in steady-state analysis.

A crucial parameter that should be obtained experimentally is the fluidity of the granular solid. We did not find experimental values in the literature, so that sensitivity of the results was investigated in order to obtain meaningful values in the simulations. The influence of γ on the pressures is not important if $\gamma \geqslant 1$ 1/kPa s, but it is very important in the computation of the velocity field. In cases where the mass flow is known, one could have good estimates of γ. Further data is very important here before one can have accurate predictions of velocities.

It was shown that both pressures on the wall and velocities inside the bulk solid depend on the discontinuity surfaces, as modified by the exponent m. This exponent ranges from 0–2 and reflects different shapes of the discontinuity surface, with the critical state moving from near to the state with lowest hydrostatic pressure to close to the state with the highest pressure.

An independent evaluation of the discontinuity surface is necessary in each case before the present viscoplastic flow model can be applied. Tests of this kind are in progress at the moment for some agricultural products (soy, rice, wheat, sunflower and sorghum) and are expected to provide independent values of the exponent m.

In the present model the results are not significantly affected by the choice of the initial viscosity μ_0 at the start of the iterations. Notice that this was a serious problem found with the original model of non-associative flow using Drucker–Prager/von-Mises, as reported by Elaskar et al. (1995).

Identification of an adequate penalty parameter α should be done in each problem, to make sure that the solution falls within a plateau. For the cases considered it was found that $\alpha \geqslant 10^7$ was adequate, even though the geometries and material properties showed large differences.

The constitutive model presented in this paper for viscoplastic flow of granular solids is more complex

than that discussed by Diez and Godoy (1992), as it includes the exponent m that should arise from experiments. The loss of simplicity has the great benefit that convergence is achieved with similar computer resources and a low number of iterations.

Models based on particle mechanics, on the other hand, may provide good estimates for the same problems, by using much larger computer resources.

Acknowledgements

The first two authors were supported by the Science Research Council of Argentina, CONICET, during the research. Grants from CONICET, the Science Research Council of Córdoba (CONICOR) and the National University of Córdoba (SECYT-UNC) supported the work carried out in Argentina. Work at West Virginia University was supported by a Grant from the U.S. Department of Energy.

References

Aris, R., 1989. Vectors, Tensors, and the Basic Equations of Fluid Mechanics. Dover, New York.

Aubrey, D., Kodaissi, E., Meimon, E., 1985. A viscoplastic constitutive equation for clays including damage law. In: Proc. 5th ICONMIG, Nagoya, vol. 1, pp. 421–428.

Bird, R.B., Armstrong, R.C., Hassager, O., 1977. Dynamics of Polymeric Liquids. In: Fluid Mechanics, vol. 1. John Wiley, New York.

Brown, R.L., Richards, J.C., 1970. Principles of Powder Mechanics. Pergamon Press, London.

Cundall, P.A., Strack, O., 1979. A discrete numerical model for granular assemblies. Geotechnique 29, 47–65.

Desai, C., Siriwardane, H., 1984. Constitutive Laws for Engineering Materials. Prentice-Hall, Englewood Cliffs, New York.

Diez, M.A., Godoy, L.A., 1992. Viscoplastic incompressible flow of frictional cohesive solids. Int. J. of Mechanical Sciences 34, 395–408.

Duvaut, G., Lions, J., 1972. Les Inequations en Mechanique et an Physique. Dunos, Paris.

Elaskar, S.A., Godoy, L.A., 1998a. Constitutive relations for compressible granular materials using non-Newtonian fluid mechanics. Int. J. Mechanical Sciences 40 (10), 1001–1018.

Elaskar, S.A., Godoy, L.A., 1998b. An application of non-Newtonian fluid mechanics to granular flow using a critical state concept. Powder Handling and Processing 10 (3), 239–244.

Elaskar, S.A., Godoy, L.A., Brewer, A.T., 1996. Granular flow based on non-Newtonian fluid mechanics. In: Lin, Y.K., Su, T.C. (Eds.), Engineering Mechanics, vol. 1. ASCE, New York, pp. 394–397.

Flavigny, E., Nova, R., 1990. Viscous properties of geomaterials. In: Darve, F. (Ed.), Geomaterials. Constitutive Equations and Modelling. Elsevier, London.

Gray, D., Stiles, J., 1988. On the Constitutive Relation for Frictional Flow of Granular Materials. Topical Report DOE/MC/21353-2584 (DE88001089), U.S. Department of Energy.

Gray, D., Stiles, J., 1990. Theoretical and Numerical Studies of Constitutive Relation for Frictional Granular Flow. Annual Report DOE/MC/24207-2852 (DE90009662), U.S. Department of Energy.

Gray, D., Stiles, J., 1991. Geometry of yield surfaces for frictional flow of granular materials. In: Mechanics Computing in 1990s and Beyond, vol. 2. ASCE, New York, pp. 1219–1223.

Gray, D., Stiles, J., Celik, I., 1991. Theoretical and Numerical Studies of Constitutive Relation for Frictional Granular Flow. Final Report DOE/MC/24207-3009 (DE91002089), U.S. Department of Energy.

Haussler, U., Eibl, J., 1984. Numerical investigation on discharging silos. J. Engineering Mechanics, ASCE 110 (6), 957–971.

Hughes, T., 1987. The Finite Element Method. Prentice-Hall, New Jersey.

Hughes, T., Liu, W., Brooks, A., 1979. Finite element analysis of incompressible viscous flows by the penalty function formulation. J. Comp. Phys. 30, 1–60.

Johnson, P., Jackson, R., 1987. Frictional–collisional constitutive relations for granular materials, with application to plane shearing. Journal of Fluid Mechanics 176, 67.

Kmita, J., 1991. An experimental analysis of internal silo loads. Bulk Solids Handling 11 (2), 459–468.

Kolymbas, D., 1994. Hypoplasticity as a constitutive framework for granular materials. In: Computer Methods and Advances in Geomechanics, vol. 1. Balkema, Rotterdam, pp. 197–208.

Lade, P., 1977. Elasto-plastic stress strain theory for cohesionless soil with curved yield surface. Int. J. Solids and Structures 13, 1019.

Lubliner, J., 1990. Plasticity Theory. Maxwell Mcmillan, New York.

Lun, C., Savage, B., Jeffery, D., Chepurniy, N., 1984. Kinetic theory for granular flow: inelastic particles in Couette flow and slightly inelastic particles in a general flow field. Journal of Fluid Mechanics 140, 223.

Mehrabadi, M., 1986. Modeling of rate-independent flow of granular materials. In: Proceedings of the X U.S. National Congress of Applied Mechanics. ASME, New York.

Nguyen, T., Brennen, C., Sabersky, R., 1979. Gravity flow of granular materials in conical hoppers. J. Applied Mechanics, ASME 46 (3), 529–535.

Ocone, R., Astarita, G., 1995. Compression and rarefaction waves in granular flow. Powder Technology 82, 231.

Oñate, E., 1986. Análisis de problemas de conformado de metales por el método de los elementos finitos utilizando una formulación de flujo viscoplásico. Mecánica Computacional, vol. 5. AMCA, 152–177 In Spanish.

Perzyna, P., 1966. Fundamental problems in viscoplasticity. In: Recent Advances in Applied Mechanics, vol. 9. Academic Press, New York, pp. 343–377.

Pitman, E., Schaeffer, D., 1987. Stability of time dependent compressible granular flow in two dimensions. Communications in Pure and Applied Mathematics 40, 421–447.

Potatov, A., Campbell, Ch., 1994. Computer Simulation of Particle Fracture and Hopper Flows. USC Report IFPRI.6. Department of Mechanical Engineering, University of Southern California.

Savage, S., 1988. Streaming motions in a bed of vibrationally fluidized dry granular materials. Journal of Fluid Mechanics 194, 457.

Schaffer, D.G., 1987. Instability in the evolution equations describing granular flow. Journal of Differential Equations 66, 19–50.

Syamalal, M., 1985. Multiphase hydrodynamics of gas–solids flow. Doctoral dissertation, Illinois Institute of Technology.

Walker, D., Blanchard, M., 1967. Pressures in experimental coal hoppers. Chemical Engineering Science 22, 1706–1713.

Zienkiewicz, O., Taylor, R., 1991. The Finite Element Method, vol. 2. McGraw-Hill, New York.